Photocatalytic Mechanisms

International Edition: DOI: 10.1002/anie.201907247
German Edition: DOI: 10.1002/ange.201907247

Unraveling the Light-Activated Reaction Mechanism in a Catalytically Competent Key Intermediate of a Multifunctional Molecular Catalyst for Artificial Photosynthesis

Linda Zedler[+], Alexander Klaus Mengele[+], Karl Michael Ziems, Ying Zhang, Maria Wächtler, Stefanie Gräfe, Torbjörn Pascher, Sven Rau, Stephan Kupfer,* and Benjamin Dietzek**

Abstract: *Understanding photodriven multielectron reaction pathways requires the identification and spectroscopic characterization of intermediates and their excited-state dynamics, which is very challenging due to their short lifetimes. To the best of our knowledge, this manuscript reports for the first time on in situ spectroelectrochemistry as an alternative approach to study the excited-state properties of reactive intermediates of photocatalytic cycles. UV/Vis, resonance-Raman, and transient-absorption spectroscopy have been employed to characterize the catalytically competent intermediate* $[(tbbpy)_2Ru^{II}(tpphz)Rh^{I}Cp^*]$ *of* $[(tbbpy)_2Ru(tpphz)Rh(Cp^*)Cl]Cl(PF_6)_2$ (***Ru(tpphz)RhCp****), *a photocatalyst for the hydrogenation of nicotinamide (NAD-analogue) and proton reduction, generated by electrochemical and chemical reduction. Electronic transitions shifting electron density from the activated catalytic center to the bridging tpphz ligand significantly reduce the catalytic activity upon visible-light irradiation.*

[*] Dr. L. Zedler,[+] Dr. Y. Zhang, Dr. M. Wächtler, Prof. Dr. B. Dietzek
Department Functional Interfaces
Leibniz Institute of Photonic Technology Jena (IPHT)
Albert-Einstein-Straße 9, 07745 Jena (Germany)
E-mail: benjamin.dietzek@leibniz-ipht.de

K. M. Ziems, Dr. Y. Zhang, Dr. M. Wächtler, Prof. Dr. S. Gräfe, Dr. S. Kupfer, Prof. Dr. B. Dietzek
Institute of Physical Chemistry and Abbe Center of Photonics
Friedrich Schiller University Jena
Helmholtzweg 4, 07743 Jena (Germany)
E-mail: stephan.kupfer@uni-jena.de
benjamin.dietzek@uni-jena.de

A. K. Mengele,[+] Prof. Dr. S. Rau
Department of Inorganic Chemistry I, University of Ulm
Albert-Einstein-Allee 11, 89081 Ulm (Germany)
E-mail: sven.rau@uni-ulm.de

T. Pascher
Pascher Instruments AB
Stora Råby Byaväg 24, S-224 80 Lund (Sweden)

[+] These authors contributed equally to the work.

Supporting information and the ORCID identification number(s) for the author(s) of this article can be found under: https://doi.org/10.1002/anie.201907247.

Introduction

Solar-driven water splitting to release molecular hydrogen as a carbon-neutral energy source is an attractive solution to satisfy the rising global energy demand.[1] Despite considerable progress, artificial photosynthesis does not reach its full potential in sustainably converting solar energy into chemical energy. Attempts to develop visible-light-driven hydrogen-evolution catalysts generally include a photosensitizer for light harvesting, an inter- or intramolecular electron relay to achieve charge separation, and a catalytic center for hydrogen generation. Many approaches for heterogeneous and homogeneous systems have been established and spectroscopically studied to elucidate the reaction mechanism and to explore the factors determining the catalytic activity.[2] However, intramolecular photocatalytic reactions often involve complex multi-step reactions with short-lived and highly reactive intermediates. Since water splitting is an inherent multielectron process, elucidation of the properties of the redox-activated intermediates is of paramount importance to understanding the overall catalytic activity. The identification of those intermediates and their excited-state processes within the electron-transfer cascades are of fundamental importance for an understanding of the catalytic mechanism and the identification of competing deactivation pathways. Therefore, detailed knowledge with respect to the structure, photophysical properties, and photoinduced dynamics of short-lived photoexcited intermediates is of utmost importance to develop highly active and stable photocatalysts for hydrogen production and other uses.

Therefore, the presented work investigates these intermediates which result from photoexcitation and subsequent electron transfer by spectroelectrochemical methods (UV/Vis absorption and resonance-Raman (rR) spectroscopy) in combination with quantum-chemical simulations.[3] rR spectroscopy is specifically suitable to identify the initially photoexcited state because only those vibrations are enhanced that are connected to structural changes coupled to the electronic transition.[4] Time-resolved transient absorption (TA) spectroelectrochemistry (SEC) enables the investigation of the photoinduced electron transfer in intermediates of the catalytic cycles on femto-to-nanosecond timescales.

Here, we combine rR- and TA-SEC with the photocatalytic characterization of a key intermediate in the photocatalytic cycle of $[(tbbpy)_2Ru(tpphz)Rh(Cp^*)Cl]Cl(PF_6)_2$ (**Ru(tpphz)RhCp***) (Figure 1 A, structure on the left).[5] The catalyst features a Ru^{II} chromophore, a tetrapyridophenazine

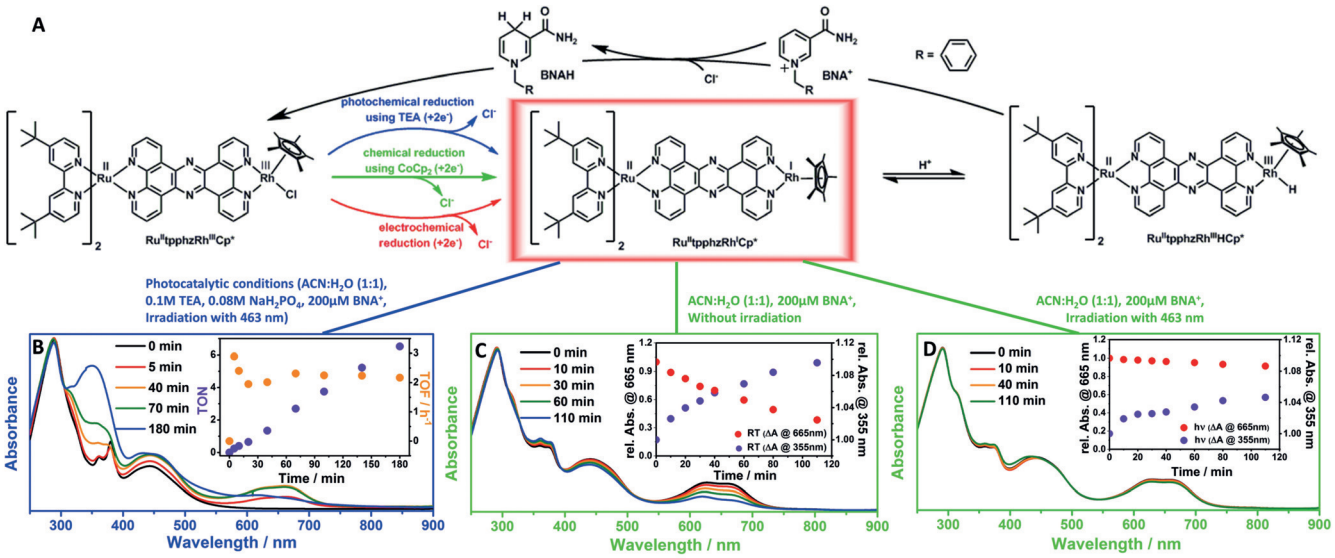

Figure 1. A) Molecular structure of the hetero-binuclear photocatalyst (left). Cleavage of the chloro ligand is observed during the $2e^-$ reduction, resulting in a Rh^I intermediate Ru^{II}(tpphz)Rh^ICp* (framed in red). The general mechanism of the light-driven catalytic hydrogenation of N-benzylnicotinamide (BNA^+ to BNAH) is displayed, including various possibilities to generate the fully charged Ru^{II}(tpphz)Rh^ICp* (blue: photocatalytic conditions; green: chemical reduction with $CoCp_2$; red: electrochemical reduction). B) UV/Vis-spectroscopic monitoring of the light-driven (λ_{exc} = 463 nm) catalytic hydrogenation of a nicotinamide using 20 µM **Ru(tpphz)RhCp*** in ACN:H_2O = 1:1 with 0.1 M TEA and 0.08 M NaH_2PO_4. Inset: Calculated catalysis parameters TON and TOF based on the spectroscopic changes at 355 nm induced by the formation of BNAH. C), D) UV/Vis-spectroscopic changes during addition of 200 µM of the subtrate BNA^+ to a solution containing chemically (by $CoCp_2$) reduced **Ru(tpphz)RhCp*** during irradiation with a 463-nm LED stick. Insets: Relative absorbance changes at 665 nm and 355 nm with time.

(tpphz) bridging ligand, and a Rh^{III}(Cp*)Cl catalytic center. In the presence of sacrificial electron donors, it photocatalytically reduces nicotine amides, which are biologically usable NAD-like (nicotinamide adenine dinucleotide) cofactors (Figure 1 A).[6] The preorganized structure of the chromophore and the catalyst prevents the formation of bioinactive NAD(P) dimers.[6,7] Additionally, catalytic hydrogen evolution was observed for more than six times longer (650 hours) than for structurally similar tpphz-bridged photocatalysts.[2c,8] However, the use of **Ru(tpphz)RhCp*** as a photocatalyst for hydrogen production shows a catalytic activity much lower than for NAD^+ reduction. Thus, the study presented here focuses on the mechanism of the light-driven reduction of NAD-like cofactors. The reductively fully activated intermediate in the respective photocatalytic cycle containing two reduction equivalents, that is, [(tbbpy)$_2$$Ru^{II}$(tpphz)$Rh^I$Cp*] (Figure 1, center), is likely formed in presence of an excess of a sacrificial electron donor upon irradiation with visible light. Here we exploit electrochemical reduction and chemical reduction with $CoCp_2$ to form this species. It should be noted that finding a suitable reductant to access the catalytically competent intermediate presents a delicate task, because the respective redox potentials have to be balanced to selectively reduce the Rh ion only, a task, however, easily accomplished by electrochemical reduction. The catalytic competence of the fully reduced **Ru(tpphz)RhCp*** towards the formation of reduced nicotine amides is shown (Figure 1).[6] To the best of our knowledge, we present, for the first time, the results of early-time photodynamics of electrochemically generated intermediates of a fully competent photocatalyst, that is, the doubly reduced **Ru(tpphz)RhCp***, under non-catalytic conditions to gain important mechanistic insights into electron-transfer cascades occurring during the catalytic cycle. These joint catalytic–spectroscopic mechanistic insights provide a detailed picture of structure–function–activity correlations in this class of photocatalysts for artificial photosynthesis.

Results and Discussion

Figure 1 schematically indicates key reaction steps underlying the light-driven multielectron proton-coupled hydrogenation of N-benzylnicotinamide (BNA^+) by **Ru(tpphz)RhCp***. To unravel mechanistic details of the reaction, specifically the photoinduced reactivity of the key intermediate (shown in the red box of Figure 1), the photocatalytic reaction was first monitored by UV/Vis spectroscopy (Figure 1 B). In a second step, the catalytically active species (Figure 1 A, center) was generated by chemical reduction with $CoCp_2$ and tested for its reactivity (Figure 1 C,D and Figure S18 in the Supporting Information). Here, irradiation of the chemically doubly reduced **Ru(tpphz)RhCp*** in presence of BNA^+ significantly hampered the catalytic turnover, as indicated by comparing the much stronger absorbance increase at 355 nm (ascribed to the formation of the reduced product BNAH) in the dark compared to the same sample under continuous irradiation with visible light. Finally, the intermediate was prepared in an electrochemical approach and characterized by UV/Vis, rR-SEC, TA-SEC, and quantum-chemical simulations. The electrochemical characterization reveals that the first and second reduction in **Ru(tpphz)RhCp*** is located at the Rh ion: The irreversible reduction at −0.6 V vs. a silver pseudo-reference electrode is due to a two-electron process in the $Rh^{III/I}$ pair (Figure 2 B,

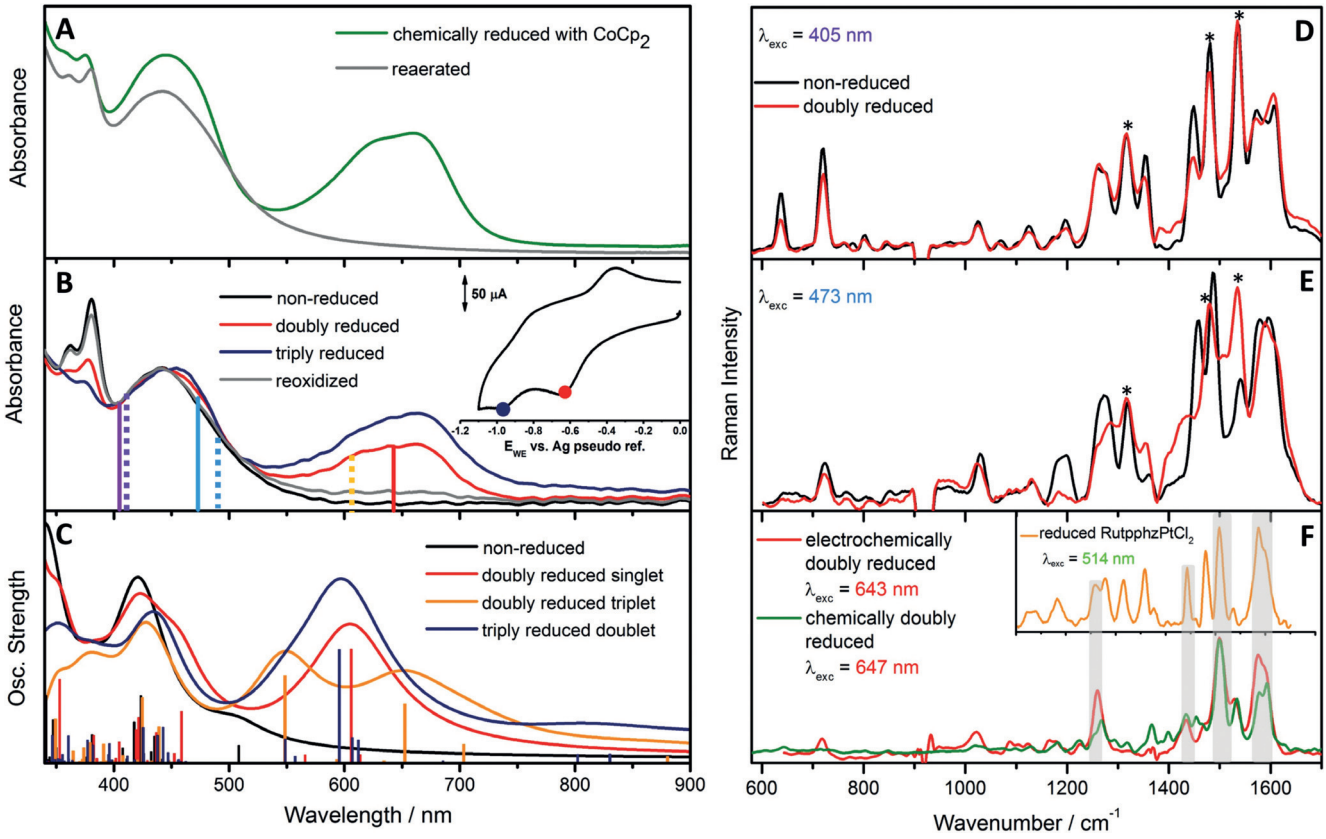

Figure 2. A) UV/Vis spectrum of the chemically reduced **Ru(tpphz)RhCp*** (green trace) using $CoCp_2$ as a reducing agent and the spectrum recorded after reaeration (grey trace) of the solution which regenerates the parent complex. B) Experimental in situ and C) calculated UV/Vis spectroelectrochemical results of the reduction states of **Ru(tpphz)RhCp***. Inset in (B): Cyclovoltammetry of **Ru(tpphz)RhCp*** in ACN containing 0.1 M $TBABF_4$ electrolyte. The applied potentials for the acquisition of the UV/Vis spectra are marked in red and blue (scan rate 100 mVs^{-1}, glassy carbon working electrode, Pt counter electrode, and Ag/AgCl pseudo-reference electrode). rR excitation and transient-absorption pump wavelengths are displayed as continuous and dashed vertical lines in the spectra, respectively. D)–F) Experimental rR spectra of non-reduced (black), electrochemically doubly reduced (red) and chemically reduced (green) **Ru(tpphz)RhCp***, excited at 405 (D), 473 (E), as well as 643 and 647 nm (F). Modes assigned to the tbbpy ligands are marked with an asterisk. Inset: rR spectrum of reduced Ru(tpphz)$PtCl_2$, excited at 514 nm, shown for comparison. Gray-shaded Raman bands are assigned to tpphz vibrations.

inset).[9] This process can be explained by two possible pathways: Either a one-electron reduction is followed by fast disproportion of the Rh^{II} intermediate,[9b] or potential inversion of the redox potential of the Rh^{II}/Rh^{I} and Rh^{III}/Rh^{II} pairs allows for an ECE (electrochemical reaction, chemical reaction, electrochemical reaction) process at the applied potential.[10] The reduction induces a loss of the chloro ligand, altering the original piano-stool geometry of the Rh^{III}(Cp*)Cl center in **Ru(tpphz)RhCp***, that is, the plane of the cyclopentadienyl ligand is now oriented perpendicular to the tpphz ligand (Figure 1A, center).[11] In analogy with previous studies, the reduction at −0.9 V is assigned to the first reduction of the tpphz ligand (Figure 2B).[5] **Ru(tpphz)RhCp*** exhibits similar absorption properties as the structurally related compounds Ru(tpphz)$PdCl_2$ and Ru(tpphz)PtX_2 (X = Cl, I).[3b,12] The different catalytic centers do not affect the steady-state absorption properties significantly.[5,13] The band at 440 nm is due to metal-to-ligand charge-transfer (MLCT) transitions from the Ru^{II} center to both the tpphz and the tbbpy ligands (Figure 2B).[12] Bands between 350 and 400 nm stem from tpphz-centered π–π* transitions, whereas the sharp band peaking at 286 nm is due to intra-ligand π–π* transitions located at the Cp* and the tbbpy moieties. Upon chemical reduction of **Ru(tpphz)RhCp*** by $CoCp_2$, a broad absorption at 650 nm arises, while the spectral changes in the other spectral regions remain minute (Figure 2A). The same was observed for the photochemical reduction of **Ru(tpphz)RhCp*** in presence of TEA (Figure S17). These reduction-induced changes are also apparent upon electrochemical reduction (Figure 2B), which can be performed at specific potentials enabling a stepwise reduction of **Ru(tpphz)RhCp***. A similar absorption feature was previously observed for singly reduced Ru(tpphz)$PtCl_2$ and assigned to an intra-ligand π–π* transition of the reduced tpphz ligand by rR-SEC and TD-DFT simulations (red line, Figure 2C).[3b] This startling coincidence can be rationalized considering that photoexcitation of the reduced **Ru(tpphz)RhCp*** may occur at the Rh^{I} center, that is, a MLCT from the Rh^{I} to the tpphz ligand occurs. Such a transition is observed in the same range as intra-ligand π–π* transitions of the reduced tpphz ligand, as evident from studies on the model complex (phen)Rh^{I}Cp*.[14] Further evidence is pro-

vided by means of quantum-chemical calculations, predicting bright MLCT transitions into the S_7 state at 606 nm (Table S4 and Figure S8) and the T_{11} state at 652 nm (Table S5 and Figure S10) for the doubly reduced **Ru(tpphz)RhCp*** within singlet and triplet multiplicity, respectively. UV/Vis-SEC during the third reduction of **Ru(tpphz)RhCp*** reveals a strong absorption increase between 500 and 800 nm, which is related to ^{2}MLCT transitions from Rh^I to the tbbpy ligands (D_{23} and D_{24}) as well as from Rh^I to the tpphz ligand (D_{25}), and to the intra-ligand π–π^* transition (D_{28}) of the now reduced tpphz ligand (blue line, Figure 2B and C, see Supporting Information for details).

To reveal structural changes of **Ru(tpphz)RhCp*** upon reduction, rR-SEC was performed at 405, 473, and 643 nm (Figure 2D–F).[3b,c,4,12,15] At 405 and 473 nm, MLCT transitions are probed which involve both the tbbpy and the tpphz ligands around the Ru^{II} center.[4,16] In line with previous studies on closely related complexes, the contribution of the tpphz ligand to the rR spectra is higher upon 473-nm excitation as compared to excitation at 405 nm (Figure 2D and E).[12–13,17]

Rh^{III}/Rh^I reduction causes only minor changes in the rR spectra of **Ru(tpphz)RhCp*** excited at 405 nm (Figure 2D): The tbbpy-assigned bands at 1320, 1480, and 1540 cm^{-1} roughly keep their intensity upon reduction, while tpphz-associated modes decrease notably. Also, the rR spectra recorded at 473 nm (Figure 2E) show an intensity increase of tbbpy-related bands, while the intensity of tpphz-associated bands diminishes. Hence, photoexcitation of the reduced **Ru(tpphz)RhCp*** at 405 and 473 nm leads to a tbbpy-MLCT being populated. Reduction of the Rh-center appears to impede a MLCT transition to the tpphz ligand. This finding agrees with the quantum-chemical calculations and a previous report[18] showing the excess charge at the Rh center to be partially delocalized on the phenanthroline fragment of the tpphz ligand (see Figure S15). This charge distribution apparently inhibits (additional) charge transfer from the Ru^{II} towards the tpphz ligand (Figure S8).

rR-SEC at 643 nm samples the reduction-induced absorption band at 650 nm, which is characteristic for the doubly reduced **Ru(tpphz)RhCp*** (Figure 2B). The rR spectrum at 643 nm is dominated by features which are neither visible upon excitation at 405 nor 473 nm (Figure 2F). Particularly, no bands associated with the tbbpy ligands are observed, pointing to the fact that the reduction-induced transition in the red part of the UV/Vis absorption spectrum does not involve excitation of the Ru^{II} center and the tbbpy ligands. Excitation of a $Rh^I \rightarrow$Cp* transition is unlikely due to the large electron density of the ligand.[9c,14] However, the 643-nm rR-SEC spectrum compares to the spectrum of reduced $Ru(tpphz)PtCl_2$ (Figure 2F, inset). $Ru(tpphz)PtCl_2$ is structurally similar to **Ru(tpphz)RhCp***, but the first reduction is localized on the tpphz ligand instead of the catalytic metal center.[3b] When comparing the 643-nm rR spectrum of the reduced **Ru(tpphz)RhCp*** with the respective spectrum of the reduced $Ru^{II}(tpphz^{\cdot-})Pt^{II}Cl_2$ excited at 514 nm, it becomes evident that the bands observed for the reduced **Ru(tpphz)RhCp*** are associated with the tpphz ligand. Hence, either a $Rh^I \rightarrow$tpphz MLCT or a tpphz intra-ligand (IL) is excited at 643 nm. The rR-SEC studies do not allow for discrimination between these two scenarios. TD-DFT simulations of the doubly reduced **Ru(tpphz)RhCp***, both in singlet and triplet multiplicity, show bright MLCT transitions from the Rh^I center to the tpphz ligand, partially mixed with a local excitation of the tpphz ligand, see S_7 (606 nm) and T_{11} (at 652 nm) in Figure 2C. Furthermore, a bright IL transition centered on the tpphz ligand (T_{21}), typical for the reduced tpphz, is predicted by TD-DFT at 548 nm for the doubly reduced triplet species.

Thus, rR-SEC shows that reduction of the Rh^{III} center in **Ru(tpphz)RhCp*** alters the electronic transitions available at the Ru^{II} photocenter, that is, the additional charge density upon Rh^{III}/Rh^I reduction becomes partially delocalized over the tpphz ligand and prohibits further charge-density shift on the bridging ligand by excitation of a $Ru^{II} \rightarrow$tpphz MLCT. For $Ru(tpphz)PtCl_2$, the transfer of the second electron, which is indispensable for hydrogen evolution at the Pt center, onto the tpphz bridging ligand is impeded by the additional charge localized on the phenazine (phz) moiety.[3b] Contrary to that, the initial localization of the excited state on the tbbpy ligands in the doubly reduced **Ru(tpphz)RhCp*** should not adversely affect the turnover at the RhCp* moiety since no third electron is required on the Rh^I center to promote typical metal-mediated catalysis.[19]

Resonance Raman experiments upon excitation at 647 nm on the chemically reduced **Ru(tpphz)RhCp*** (see Figure 2F) yield identical band pattern as the corresponding experiment on the electrochemically reduced catalysts. Together with the striking similarities of the respectively generated UV/Vis spectra (Figure 2A and B), this provides clear evidence that both approaches yield the same product, that is, $[(tbbpy)_2Ru^{II}(tpphz)Rh^ICp^*]$. Furthermore, UV/Vis spectroscopic investigations also confirms the similarity of the electrochemically and photochemically generated doubly reduced **Ru(tpphz)RhCp*** (Figures 1, 2A, and S17).

Evaluating the Catalytic Competences of $(tbbpy)_2Ru^{II}(tpphz)Rh^ICp^*$

The reactivity of $Ru^{II}(tpphz)Rh^ICp^*$ towards the hydrogenation of N-benzylnicotinamide (BNA^+ to BNAH) can be monitored by the increased absorbance of the product around 355 nm (Figure 1B).[6] Here, we generated the "fully charged" $Ru^{II}(tpphz)Rh^ICp^*$ by chemical reduction with $CoCp_2$. Upon reaction with BNA^+ in the dark, formation of BNAH is apparent by an increased absorbance around 355 nm, the loss of absorbance of the Rh^I-tpphz MLCT band around 650 nm verified the re-oxidation of Rh^I to Rh^{III} (Figure 1C). Performing the same reaction under irradiation with an LED at $\lambda = 463 \pm 12$ nm (45 mW cm^{-2}) showed only insignificant changes of the absorption both at 650 and 340 nm (Figure 1D), that is, no signs for catalytic hydrogenation are observed.

Thus, we conclude that irradiation of the sample obviously impairs the competence of the catalyst and limits its overall efficiency. To identify and trace the deactivation pathway of the fully charged and competent catalytic species during

irradiation, transient-absorption experiments will be discussed in the following.

Femtosecond Time-Resolved Transient-Absorption Spectroelectrochemistry

Time-resolved transient-absorption experiments investigating the light-induced electron-transfer dynamics on timescales of sub-ps to ns are performed as TA-SEC measurements using pump wavelengths of 403, 492, and 600 nm. At 403 and 492 nm, both the parent and the doubly reduced **Ru(tpphz)RhCp*** complex absorb (see Figure 2B). The parent complex shows transient-absorption features reminiscent of those observed for related $[(tbbpy)_2Ru(tpphz)MX_2]^{2+}$ ($MX_2 = PdCl_2$, $PtCl_2$, PtI_2) upon MLCT excitation:[2d,13,17] An instantaneous bleaching of the ^{1}MLCT band reflects the shift of electron density from the Ru^{II} to both tbbpy and tpphz ligands (Figure 3A). In the latter case, the phenanthroline (phen) moiety serves as the primary electron-density acceptor. The 1-ps process contains contributions from ^{1}MLCT→^{3}MLCT intersystem crossing (ISC), vibrational relaxation, and an inter-ligand charge transfer (ILCT) from the tbbpy moiety to the phenanthroline part of the tpphz ligand (Figures 2D and S16) (Due to the limited temporal resolution and the spectral congestion of the processes, the individual contributions cannot be resolved). The phenanthroline-centered state relaxes into a phenazine-centered ^{3}MLCT state ($\tau_2 = 11$ ps), which decays with a lifetime of 450 ps (τ_3; Figures 3D and S16). The assignment of the phenazine-centered ^{3}MLCT state is based on the broad absorption of the phenazine radical anion at about 590 nm, which builds up within 20 ps concomitantly with a slight blue-shift of the absorption maximum (Figure 3A).

Further evidence for the origin of the excited-state absorption (ESA) at 590 nm is provided by TD-DFT calculations addressing the absorption by spin-allowed triplet–triplet excitations, which reveal a bright ^{3}IL transition at 609 nm centered on the phenazine moiety (see T_{27} in Figure 3B). This absorption subsequently loses intensity, in particular the blue part of the band (Figure 3A and C).

As a result, the 450-ps component in the decay-associated spectra (DAS) shows no intensity towards the near IR, while the infinite-time spectrum appreciably absorbs at 750 nm (Figure 3D). This feature indicates electron transfer from the formally reduced phenazine species towards the catalytic Rh^{III} center: TD-DFT reveals that the $[(tbbpy)_2Ru^{III}(tpphz)Rh^{II}Cp^*]$ species shows appreciable absorption at 738 nm due to a bright Rh^{II}→tpphz ^{3}MLCT (T_{12}), while $[(tbbpy)_2Ru^{III}tpphz^{\bullet-}Rh^{III}Cp^*Cl]$ strongly absorbs at around 600 nm, based on the ^{3}IL excitation into T_{27} (Figure 3B). These results explain the spectral shape of the visible excited-state absorption reflected in the DAS of the τ_3- and the long-lived component (Figure 3D).

The excellent match between the experimentally obtained DAS and the calculated spectra indicates not only electron transfer from the photoactive $[(tbbpy)_2Ru^{II}(tpphz)]$ fragment to the catalytically active Rh center, it also confirms Cl^- dissociation on the 450 ps timescale upon metal-centered

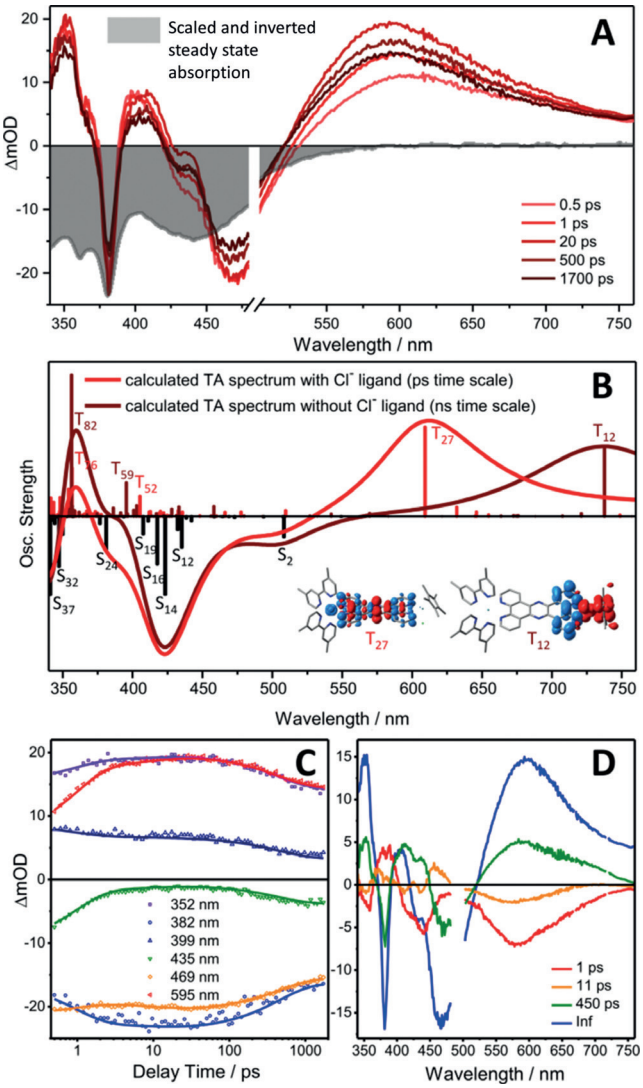

Figure 3. Transient-absorption data including A) experimental and B) calculated transient-absorption spectra at selected delay times, C) transient kinetics at key wavelengths, and D) spectral changes associated with each kinetic process (DAS) for non-reduced **Ru(tpphz)RhCp*** pumped at 492 nm. For comparison, the inverted (that is, negative) steady-state absorption of the complex **Ru(tpphz)RhCp*** is also plotted (in gray) and scaled to the largest ground-state bleach signal at 360 nm (A). Inset in (B): Charge-density differences for bright spin-allowed triplet–triplet excitations into intra-ligand State T_{27} (with Cl^-) and into metal-to-ligand charge-transfer state T_{12} (without Cl^-); charge transfer takes place from red to blue.

one-electron reduction.[20] Notably, structural reorganization at the reduced Rh^{II} center upon Cl^- dissociation leads to a linear tpphz-Rh-Cp* geometry in which the Rh^{II} center is shielded by steric and electronic factors from geminate recombination with the solvated Cl^-, hence leading to the long-lived species and, as a consequence, to the long-lived red-absorbing component in the transient absorption (blue infinite-time component in the DAS, Figures 3D and S16). In a recent report, this slow decay of the Rh^{II} species has been shown to obey second-order kinetics, which was interpreted as a disproportionation reaction yielding Rh^{I} and Rh^{III} in the μs-to-ms time range.[21]

After the two-electron reduction of **Ru(tpphz)RhCp*** accompanied by Cl^- dissociation from the pentamethylcyclopentadienyl-Rh^{III} center,[11,22] the photodynamics of $[(tbbpy)_2Ru^{II}(tpphz)Rh^{I}Cp^*]$, that is, the photoinduced processes in a "fully charged" molecular photocatalyst, are observed (Figure 4). To the best of our knowledge, the data discussed in the following present the first ultrafast-transient-absorption study on an isolated molecular photocatalyst in its fully active electronic configuration.

As discussed in the context of the rR data, excitation of $[(tbbpy)_2Ru^{II}(tpphz)Rh^{I}Cp^*]$ at 403 nm populates a MLCT state in which electron density is shifted to the tbbpy ligands, that is, $[(tbbpy)(tbbpy^{\bullet-})Ru^{III}(tpphz)Rh^{I}Cp^*]$ is formed (Scheme 1). The ESA at 360 nm reflects intra-ligand absorption of the tbbpy radical anion (Figure 4 A). Nonetheless, photoexcitation leads to an instantaneous (within the experimental time resolution) and rather strong bleach signal at 650 nm, which is assigned to a $Rh^{I}\rightarrow$tpphz MLCT transition based on TD-DFT and UV/Vis-SEC results (Figures 2 B,C and 4 A). This feature thus indicates an interaction between the two metal centers and a hole transfer from the photoexcited Ru^{III} center to the Rh^{I} center. This process occurs rapidly, that is, below 500 fs, and leads to the formation of $[(tbbpy)(tbbpy^{\bullet-})Ru^{II}(tpphz)Rh^{II}Cp^*]$. This state is initially vibrationally hot and cools down with the time constant $\tau_1 = 1.8$ ps. Cooling causes a slight shift of both the ESA maxima at 470 nm and the $\Delta OD = 0$ crossing at 725 nm (Figure 4 A). The relaxed $[(tbbpy)(tbbpy^{\bullet-})Ru^{II}(tpphz)Rh^{II}Cp^*]$ reveals a strong ESA above 720 nm, which the calculations assign to a tpphz$\rightarrow Rh^{II}$-LMCT transition. In addition to the $tbbpy^{\bullet-}$ absorption below 440 nm, the bleaching of the $Rh^{I}\rightarrow$tpphz MLCT transition at around 630 nm is apparent (Figure 4 A). The strong bleaching of the signal at about 480 nm (Ru^{II} center) is not visible in DAS (τ_1) and DAS (τ_2) but only appears on a 100 ps timescale. On this timescale, associated with $\tau_2 = 43$ ps, inter-ligand $tbbpy^{\bullet-}\rightarrow$tpphz electron transfer takes place, that is, $[(tbbpy)_2Ru^{II}(tpphz^{\bullet-})Rh^{II}Cp^*]$ is formed (Scheme 1). We hypothesize that the partial bleaching of the signal associated with the Ru center in $[(tbbpy)(tbbpy^{\bullet-})Ru^{II}(tpphz)Rh^{II}Cp^*]$ is superimposed by a $tbbpy^{\bullet-}\rightarrow$tpphz excited-state absorption. This renders the net optical-density changes in the spectral region below 500 nm slightly positive. Upon inter-ligand $tbbpy^{\bullet-}\rightarrow$tpphz electron transfer, more prominent GSB features below 500 nm are observed, while the bleaching of the signal associated with the Rh center at 650 nm decreases (Figure 4 A). Interestingly, the inter-ligand charge transfer process is relatively slow compared to inter-ligand hopping processes observed in Ru^{II} complexes and the non-reduced parent **Ru(tpphz)RhCp*** (11 ps), which is attributed to the fact that electron density in the Rh^{II} center partially extends towards the tpphz-bridging ligand, as indicated by the respective spin density in Figure S15. Hence, the additional negative charge on the phenanthroline fraction of the tpphz ligand coordinating the Rh ion slows down the kinetics of inter-ligand electron transfer towards the bridging ligand. With the characteristic time constant of $\tau_3 = 600$ ps, the excess charge density on the tpphz ligand shifts to the lowest orbital available, that is, from the phenanthroline to the phenazine moiety of the bridging ligand. This is manifested in the comparably low negative ΔOD amplitude at around 630 nm, which stems from the superposition of the Rh-center ground-state bleach and the excited-state absorption of the reduced tpphz ligand, more specifically the reduced central phenazine unit (DAS, Figure 4 A).[23] The resultant $[(tbbpy)_2Ru^{II}(phen\text{-}phz^{\bullet-}\text{-}phen)Rh^{II}Cp^*]$, bearing the electron in the central phenazine moiety, forms the long-lived species which decays back to the ground state with a time constant beyond the experimentally accessible time range (Scheme 1).

The slow ns-decay component observed in the TA-SEC data upon 403-nm excitation corresponds to the intramolecular electron transfer of the second electron onto a mono-reduced catalytic Rh^{II} center. This electron-transfer step is apparently much slower than the corresponding first electron

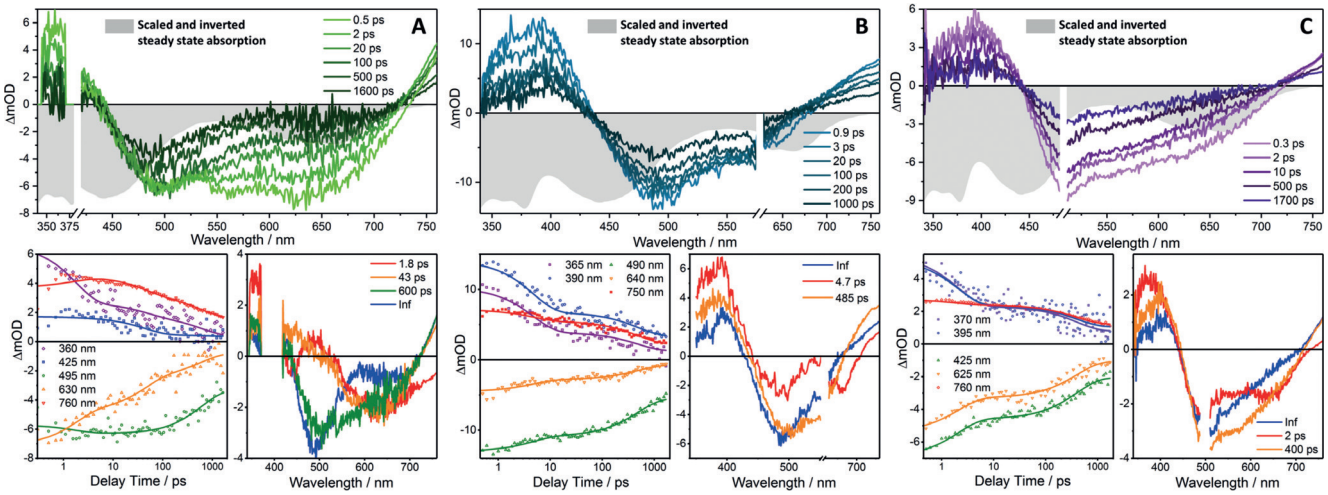

Figure 4. Transient-absorption data including transient absorption spectra at selected delay times, transient kinetics at key wavelengths, and spectral changes associated with each kinetic process (DAS) for doubly reduced **Ru(tpphz)RhCp*** pumped at A) 403, B) 600, and C) 492 nm. For comparison, the inverted, (that is, negative) steady-state absorption spectra of doubly reduced **Ru(tpphz)RhCp*** are also plotted (in gray) and scaled to the maximum ground-state bleach signal within the individual graphs.

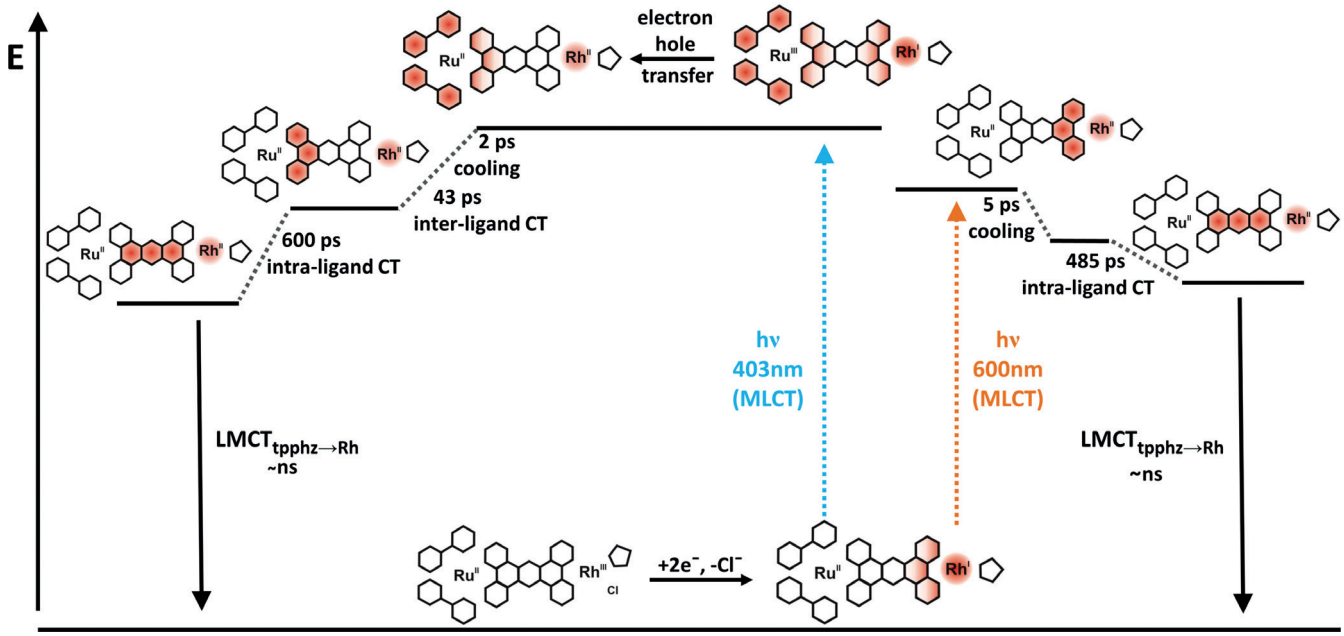

Scheme 1. Schematic representation of the proposed photophysical pathways for the doubly reduced photocatalyst **Ru(tpphz)RhCp*** upon photoexcitation at 403 and 600 nm. At 403 nm, a MLCT from Ru^{II} to the tbbpy ligand occurs, after which an electron hole is transferred on a sub-500-fs timescale, reducing Ru^{III} and oxidizing the Rh^{I} center. This process is followed by an inter-ligand transition to tpphz, finally decaying by an intra-ligand charge transfer from the phenanthroline to the phenazine fragment of the bridging ligand, followed by a MLCT to the ground state. In contrast, at 600-nm excitation, a MLCT from Rh^{I} to tpphz occurs which decays via an intra-ligand charge transfer to the ground state. Here, the Ru center and the tbbpy ligands are not involved in the photodynamic processes.

transfer in the $Rh^{III} \rightarrow Rh^{II}$ reduction (450 ps, see Figure 4 A). Since the electrochemical analysis showed a potential inversion of the Rh^{III}/Rh^{II} and Rh^{II}/Rh^{I} reduction, the slowed-down electron transfer must be attributed to the change in the relative orientation between the tpphz bridging ligand and the Cp* ligand, which results in a kinetic barrier for the electron-transfer process.

As concluded from the TA measurements and the quantum-chemical calculations, a perpendicular arrangement between the tpphz bridge and the Cp* ligand also exists in the $[(tbbpy)_2Ru^{II}(tpphz)Rh^{II}Cp^*]$ state (Figure S16). Similar to the Rh^{I} species, electron-density redistribution from the strong donor ligand Cp* over the connecting Rh^{II} core to the phenanthroline moiety of the tpphz ligand might establish an electronic barrier for the electron localized at the phenazine moiety which drastically reduces the transfer kinetics of the second electron at the catalytic unit. 600-nm excitation of the "fully charged" **Ru(tpphz)RhCp*** photocatalysts allows for a cross-validation of the model put forward before.

Excitation within the reduction-induced absorption band (see Figure 2 B) leads to a charge-density shift associated with a $Rh^{I} \rightarrow$tpphz MLCT transition. TD-DFT calculations show that the excess charge density is localized on the phenanthroline part of the bridging ligand that coordinates the Rh^{I} ion. Hence, 600-nm excitation of the doubly reduced **Ru(tpphz)RhCp*** catalyst initially leads to a vibrationally hot $[(tbbpy)_2Ru^{II}(phen\text{-}phz\text{-}phen^{\bullet-})Rh^{II}Cp^*]$ state (Scheme 1). The subsequent dynamics are characterized by a 4.7- and a 485-ps process (DAS, Figure 4 B), which lead to the population of a molecular species that outlives the experimentally accessible delay-time window of 1.8 ns. The fastest component, $\tau_1 = 4.7$ ps, is spectrally characterized by a blue-shift of the $\Delta OD = 0$ crossing at around 680 nm and the disappearance of a negative shoulder at the red-edge of the Rh^{I}-ground-state bleach (Figure 4 B). Hence, it is associated with a cooling of the $[(tbbpy)_2Ru^{II}(phen\text{-}phz\text{-}phen^{\bullet-})Rh^{II}Cp^*]$ state. However, it should be noted that the excess electron density on the tpphz ligand is still considered to be localized on the phenanthroline moiety. Only during the process associated with $\tau_2 = 485$ ps, the charge density relaxes to the central phenazine part of the tpphz ligand by forming the species $[(tbbpy)_2Ru^{II}(phen\text{-}phz^{\bullet-}\text{-}phen)Rh^{II}Cp^*]$ (Scheme 1). This species is found to be long-lived on the time scale of the femtosecond-transient-absorption experiment.

It should be pointed out that the formation of $[(tbbpy)_2Ru^{II}(phen\text{-}phz^{\bullet-}\text{-}phen)Rh^{II}Cp^*]$ occurs with a charge-density shift from the Rh^{I} fragment upon 600-nm excitation with a time constant of 485 ps, and from the Ru^{II} fragment upon 403-nm excitation with a time constant of 600 ps (Figure 4 A,B). The similarity of the characteristic timescales reflects the apparent energetic symmetry of the tpphz ligand even though it coordinates two different metal ions. In either of these cases, the phenanthroline→phenazine charge-density shift is spectrally manifested in an apparent decrease of the ground-state bleach in the red part of the $\Delta OD < 0$ band. This is due to the fact that the $phz^{\bullet-}$ fragment strongly absorbs at around 550 nm, that is, partially overriding the ground-state bleach in the same spectral region (Figures 4 A,B).[23]

Photoexcitation of doubly reduced **Ru(tpphz)RhCp*** at 492 nm leads to similar transient-absorption features ob-

tained with 403-nm excitation (Figure 4C). In agreement with rR-SEC at 473 nm, a Ru^{II}→tbbpy MLCT state is initially populated (Figures 2E and 4C). Additionally, a Rh^{I}→tpphz MLCT transition occurs, since both absorption features are spectrally broad and overlapping. Consequently, two overlapping decay processes from both MLCT transitions are observed in parallel. Therefore, the TA spectra obtained at 403- and 492-nm excitation are qualitatively similar, but their interpretation is significantly complicated. Therefore, the data was not analyzed in detail, because too many decay constants would be required, rendering an in-depth kinetic analysis unreliable.

The combined catalytic, photophysical, electrochemical and theoretical data paint a very similar picture, that is, photoexcitation of the "fully charged" **Ru(tpphz)RhCp*** complex containing a Rh^{I} ion leads to the photochemical formation of a Rh^{II} intermediate. The same light required for the photochemical generation of the catalytically competent Rh^{I} state thus leads to its deactivation by MLCT formation. This is directly reflected by the absence of catalytic activity of the intermediate **Ru^{II}(tpphz)Rh^{I}Cp*** under irradiation. The photoinduced discharging produces a relatively long-lived Rh^{II} state describing, for the first time, the catalytic inactivity of a mono-reduced (N,N)RhCp* complex, that is, the Rh^{II} state, towards nicotinamide reduction. This is particularly important because the electrochemical properties of virtually all (N,N)RhCp* complexes only permit experimental access to the directly generated Rh^{I} state during metal-centered reduction. Based on our mechanistic conclusions, we suggest — in the absence of available protons — controlling the overall catalytic process by sequential photochemical Rh^{I} generation and thermal consumption of Rh^{I} coupled to substrate conversion. Utilizing this approach, BNAH formation was successfully implemented (see Figure S19).

Conclusion

The elucidation of multi-electron reaction pathways, for example, in hydrogen-evolving photocatalysis, requires the identification and dynamic monitoring of intermediates, which can be mimicked by sequential electroreduction. To the best of our knowledge, we presented, for the first time, the results of in-situ early-time photodynamics of an isolated, molecular photocatalyst in its active electronic configuration. Pulsed laser excitation of doubly reduced **Ru(tpphz)RhCp*** at either 403 or 600 nm leads to a charge-density shift towards the central phenazine part of the bridging tpphz ligand, irrespective of the fact that completely different states are initially populated. At 403 nm, a Ru^{II}→tbbpy MLCT transition occurs, while at 600 nm, a Rh^{I}→tpphz MLCT state is populated, as confirmed by rR-SEC and TD-DFT. The long-lived radical anion $[(tbbpy)_2Ru^{II}(tpphz^{\bullet-})Rh^{II}Cp^*]$ in the described relaxation cascade is possibly a potent precursor for an additional chemical deactivation pathway of the catalyst.[24] The investigations towards the effect of blue-light irradiation of the catalytic reaction mixture containing BNA^+ clearly showed that once the doubly reduced **Ru(tpphz)RhCp*** state is formed, photoexcitation impedes the catalytic hydrogenation of BNA^+ to BNAH. This is in full agreement with the results of the detailed spectroscopic and theoretical investigation which point to the formation of an inactive Rh^{II} intermediate upon photoexcitation. The excitation-induced charge redistribution in the doubly reduced **Ru(tpphz)RhCp*** can be formally viewed as a Rh^{I}→Rh^{II} discharging process leading to the inactivation of the catalytic center. However, the actual "H"-transferring species in RhCp* catalysts is either a $Rh^{I}(Cp^*H)$[19b,25] or a $Rh^{III}(Cp^*)H$[19a,26] unit, formed upon fast[26] oxidative addition of a proton to the Rh^{I}Cp* moiety. Since this hydride-transferring agent does not exhibit a red absorbance,[19b] it is possible in these systems to escape the potential visible-light-driven inactivation of catalysis by working in sufficiently acidic media.

With respect to future applications of molecular catalysts using the whole solar spectrum for light-driven catalysis, the detected MLCT transitions from the reductively fully activated catalytic center back to the bridging ligand presumptively represent an activity-limiting step. It is clear that a more careful design of the ligand moiety supporting the catalytic center is crucial for supporting sufficiently high activity. The presented results clearly show that the design of photocatalytically active systems will benefit from close interactions between spectroscopy, theory, and synthesis, leading to the spectroscopy-aided design of next generation catalysts.

Experimental Section

Ru(tpphz)RhCp* was synthesized as described in the literature.[5] UV/Vis-SEC, rR-SEC, and electrochemical measurements were performed as described in detail in the Supporting Information. A custom-built setup was utilized to acquire fs-TA data (Pascher Instruments AB).[28] Comprehensive experimental and computational details and methods can be found in the Supporting Information.

Acknowledgements

This work was financially supported by the German Science Foundation (DI1517/11-1 and CATALIGHT CRC/RR 234, projects A1 and C5, Projektnummer 364549901). We thank the Thuringian State Government for financial support within the ACP Explore project. A.K.M. acknowledges financial support from the FCI (via a Chemiefonds-Stipendium). Y.Z. acknowledges support by the German Academic Exchange Service. K.M.Z. acknowledges support from the Konrad Adenauer foundation and the German Academic Scholarship Foundation.

Conflict of interest

The authors declare no conflict of interest.

Keywords: enzyme catalysis · rhodium · ruthenium · spectro-electrochemistry · ultrafast spectroscopy

How to cite: *Angew. Chem. Int. Ed.* **2019**, *58*, 13140 – 13148
Angew. Chem. **2019**, *131*, 13274 – 13282

[1] N. S. Lewis, D. G. Nocera, *Proc. Natl. Acad. Sci. USA* **2006**, *103*, 15729 – 15735.
[2] a) E. S. Andreiadis, M. Chavarot-Kerlidou, M. Fontecave, V. Artero, *Photochem. Photobiol.* **2011**, *87*, 946 – 964; b) J. L. Dempsey, A. J. Esswein, D. R. Manke, J. Rosenthal, J. D. Soper, D. G. Nocera, *Inorg. Chem.* **2005**, *44*, 6879 – 6892; c) S. Rau, B. Schafer, D. Gleich, E. Anders, M. Rudolph, M. Friedrich, H. Gorls, W. Henry, J. G. Vos, *Angew. Chem. Int. Ed.* **2006**, *45*, 6215 – 6218; *Angew. Chem.* **2006**, *118*, 6361 – 6364; d) Y. Halpin, M. T. Pryce, S. Rau, D. Dini, J. G. Vos, *Dalton Trans.* **2013**, *42*, 16243 – 16254.
[3] a) A. Koch, D. Kinzel, F. Dröge, S. Gräfe, S. Kupfer, *J. Phys. Chem. C* **2017**, *121*, 16066 – 16078; b) L. Zedler, J. Guthmuller, I. Rabelo de Moraes, S. Kupfer, S. Krieck, M. Schmitt, J. Popp, S. Rau, B. Dietzek, *Chem. Commun.* **2014**, *50*, 5227 – 5229; c) L. Zedler, S. Kupfer, I. R. de Moraes, M. Wächtler, R. Beckert, M. Schmitt, J. Popp, S. Rau, B. Dietzek, *Chem. Eur. J.* **2014**, *20*, 3793 – 3799; d) M. Staniszewska, S. Kupfer, J. Guthmuller, *Chem. Eur. J.* **2018**, *24*, 11166 – 11176; e) M. Martynow, S. Kupfer, S. Rau, J. Guthmuller, *Phys. Chem. Chem. Phys.* **2019**, *21*, 9052 – 9060.
[4] M. Wächtler, J. Guthmuller, L. González, B. Dietzek, *Coord. Chem. Rev.* **2012**, *256*, 1479 – 1508.
[5] A. K. Mengele, S. Kaufhold, C. Streb, S. Rau, *Dalton Trans.* **2016**, *45*, 6612 – 6618.
[6] A. K. Mengele, G. M. Seibold, B. J. Eikmanns, S. Rau, *ChemCatChem* **2017**, *9*, 4369 – 4376.
[7] A. K. Mengele, S. Rau, *Inorganics* **2017**, *5*, 35.
[8] a) M. G. Pfeffer, C. Pehlken, R. Staehle, D. Sorsche, C. Streb, S. Rau, *Dalton Trans.* **2014**, *43*, 13307 – 13315; b) M. G. Pfeffer, B. Schafer, G. Smolentsev, J. Uhlig, E. Nazarenko, J. Guthmuller, C. Kuhnt, M. Wächtler, B. Dietzek, V. Sundström, S. Rau, *Angew. Chem. Int. Ed.* **2015**, *54*, 5044 – 5048; *Angew. Chem.* **2015**, *127*, 5132 – 5136; c) M. G. Pfeffer, T. Kowacs, M. Wächtler, J. Guthmuller, B. Dietzek, J. G. Vos, S. Rau, *Angew. Chem. Int. Ed.* **2015**, *54*, 6627 – 6631; *Angew. Chem.* **2015**, *127*, 6727 – 6731.
[9] a) U. Kölle, M. Grützel, *Angew. Chem. Int. Ed. Engl.* **1987**, *26*, 567 – 570; *Angew. Chem.* **1987**, *99*, 572 – 574; b) U. Kölle, B.-S. Kang, P. Infelta, P. Comte, M. Grätzel, *Chem. Ber.* **1989**, *122*, 1869 – 1880; c) S. Chardon-Noblat, S. Cosnier, A. Deronzier, N. Vlachopoulos, *J. Electroanal. Chem.* **1993**, *352*, 213 – 228.
[10] J. A. Hopkins, D. Lionetti, V. W. Day, J. D. Blakemore, *Organometallics* **2019**, *38*, 1300 – 1310.
[11] H. Nakai, K. Jeong, T. Matsumoto, S. Ogo, *Organometallics* **2014**, *33*, 4349 – 4352.
[12] S. Tschierlei, M. Karnahl, M. Presselt, B. Dietzek, J. Guthmuller, L. González, M. Schmitt, S. Rau, J. Popp, *Angew. Chem. Int. Ed.* **2010**, *49*, 3981 – 3984; *Angew. Chem.* **2010**, *122*, 4073 – 4076.
[13] M. Wächtler, J. Guthmuller, S. Kupfer, M. Maiuri, D. Brida, J. Popp, S. Rau, G. Cerullo, B. Dietzek, *Chem. Eur. J.* **2015**, *21*, 7668 – 7674.
[14] Y. Peng, M. V. Ramos-Garcés, D. Lionetti, J. D. Blakemore, *Inorg. Chem.* **2017**, *56*, 10824 – 10831.
[15] S. Kupfer, J. Guthmuller, S. Losse, S. Rau, B. Dietzek, J. Popp, L. González, *Phys. Chem. Chem. Phys.* **2011**, *13*, 15580 – 15588.
[16] A. B. Myers, *J. Raman Spectrosc.* **1997**, *28*, 389 – 401.
[17] S. Tschierlei, M. Presselt, C. Kuhnt, A. Yartsev, T. Pascher, V. Sundström, M. Karnahl, M. Schwalbe, B. Schafer, S. Rau, M. Schmitt, B. Dietzek, J. Popp, *Chem. Eur. J.* **2009**, *15*, 7678 – 7688.
[18] M. Ladwig, W. Kaim, *J. Organomet. Chem.* **1991**, *419*, 233 – 243.
[19] a) H. C. Lo, C. Leiva, O. Buriez, J. B. Kerr, M. M. Olmstead, R. H. Fish, *Inorg. Chem.* **2001**, *40*, 6705 – 6716; b) L. M. A. Quintana, S. I. Johnson, S. L. Corona, W. Villatoro, W. A. Goddard, M. K. Takase, D. G. VanderVelde, J. R. Winkler, H. B. Gray, J. D. Blakemore, *Proc. Natl. Acad. Sci. USA* **2016**, *113*, 6409 – 6414.
[20] S. Berger, J. Fiedler, R. Reinhardt, W. Kaim, *Inorg. Chem.* **2004**, *43*, 1530 – 1538.
[21] S. Fukuzumi, T. Kobayashi, T. Suenobu, *Angew. Chem. Int. Ed.* **2011**, *50*, 728 – 731; *Angew. Chem.* **2011**, *123*, 754 – 757.
[22] T. Scheiring, J. Fiedler, W. Kaim, *Organometallics* **2001**, *20*, 1437 – 1441.
[23] M. Fujita, A. Ishida, T. Majima, S. Takamuku, *J. Phys. Chem.* **1996**, *100*, 5382 – 5387.
[24] a) M. P. Juliarena, R. O. Lezna, M. R. Feliz, G. T. Ruiz, S. Thomas, G. Ferraudi, I. Carmichael, *J. Org. Chem.* **2006**, *71*, 2870 – 2873; b) D. A. McGovern, A. Selmi, J. E. O'Brien, J. M. Kelly, C. Long, *Chem. Commun.* **2005**, 1402 – 1404.
[25] C. L. Pitman, O. N. L. Finster, A. J. M. Miller, *Chem. Commun.* **2016**, *52*, 9105 – 9108.
[26] S. I. Johnson, H. B. Gray, J. D. Blakemore, W. A. Goddard III, *Inorg. Chem.* **2017**, *56*, 11375 – 11386.
[27] a) S. A. Rommel, D. Sorsche, M. Fleischmann, S. Rau, *Chem. Eur. J.* **2017**, *23*, 18101 – 18119; b) S. Kupfer, *Phys. Chem. Chem. Phys.* **2016**, *18*, 13357 – 13367.
[28] R. Siebert, D. Akimov, M. Schmitt, A. Winter, U. S. Schubert, B. Dietzek, J. Popp, *ChemPhysChem* **2009**, *10*, 910 – 919.

Manuscript received: June 11, 2019
Accepted manuscript online: July 26, 2019
Version of record online: August 19, 2019

